New half-life limits on double-β decays of ^{110}Pd and ^{102}Pd into excited states

Björn Lehnert* and Kai Zuber†
Institut für Kern- und Teilchenphysik, Technische Universität Dresden, Dresden, Germany

Erica Andreotti‡ and Mikael Hult§
Institute for Reference Materials and Measurements, Retieseweg 111, B-2440 Geel, Belgium

(Received 10 December 2012; published 8 March 2013)

Background: Excited-state transitions in double-β decays are a powerful tool to validate and tune calculations of nuclear matrix elements.
Purpose: The experimental lower half-life limits for double-β decays of ^{110}Pd and ^{102}Pd into the excited 2_1^+ and 0_1^+ states are improved. Furthermore, the first limits of transitions into the 2_2^+, 0_2^+, and 2_3^+ states are published for ^{110}Pd as well as a first limit for the 2_2^+ state transition in ^{102}Pd.
Methods: The Pd sample was measured with two HPGe detectors in sandwich configuration in the HADES underground laboratory during 44.77 d of lifetime. The analysis was performed with the frequentist Feldman-Cousins method.
Results: Lower half-life limits of 1.98×10^{20} and 1.72×10^{20} yr (95% CL) were found for the first 0^+ and 2^+ excited states in ^{110}Pd, respectively. This is an improvement by more than a factor of 3 with respect to previous measurements. In ^{102}Pd, the lower half-life limit could be improved to 5.95×10^{18} yr (95% CL) for the first 0^+ excited state. Furthermore, first experimental lower half-life limits were found for all possible excited states in the ^{110}Pd and ^{102}Pd systems.
Conclusions: Previous half-life limits were improved and experimental results were obtained for all theoretical calculations of palladium double-β decays into excited states.

DOI: 10.1103/PhysRevC.87.034312 PACS number(s): 21.10.Tg, 23.40.Hc, 27.60.+j

I. INTRODUCTION

Groundbreaking progress has been made in the field of neutrino physics in recent years. Oscillation experiments studying neutrinos coming from the sun [1–3], the atmosphere [4], nuclear reactors [5–8], and accelerator beams [9–11] have found compelling evidence for flavor oscillation in the lepton sector. This changes the long-believed assumption that neutrinos are massless particles. The implication from neutrino oscillation that at least two neutrino mass eigenstates have a nonzero rest mass does not allow the fixing of an absolute mass scale and leaves two mass hierarchy scenarios open. Advanced oscillation experiments try to identify the hierarchy scenario by using oscillation effects in the earth or in dense stellar matter [12] but are not able to determine the absolute mass scale. This has to be done via β decay [13,14], cosmology [15], or neutrinoless double-β decay:

$$(Z, A) \rightarrow (Z + 2, A) + 2e^- \quad (0\nu\beta\beta), \tag{1}$$

which would have a high sensitivity to determine the mass scale of neutrinos. This process violates total lepton number by two units and thus is not allowed in the standard model. Furthermore, it is the gold-plated process that distinguishes whether neutrinos are Majorana or Dirac particles.

For the $0\nu\beta\beta$ process to exist, it is necessary to match the helicities of the intermediate neutrino states, which is most easily done by introducing a neutrino mass. This mass is connected to the experimentally observable half-life via

$$\left(T_{1/2}^{0\nu}\right)^{-1} = G^{0\nu}(Q, Z) \left| M_{GT}^{0\nu} - M_F^{0\nu} \right|^2 \left(\frac{\langle m_{\nu_e} \rangle}{m_e} \right)^2, \tag{2}$$

where $\langle m_{\nu_e} \rangle$ is the effective Majorana neutrino mass given by the coherent sum over the virtual electron neutrino mass eigenstates $\langle m_{\nu_e} \rangle = |\sum_i U_{ei}^2 m_i|$, with U_{ei} as the lepton flavor mixing matrix; $G^{0\nu}(Q, Z)$ is a phase space factor; and $M_{GT}^{0\nu} - M_F^{0\nu}$ describes the nuclear transition matrix element. The experimental signature is the emission of two electrons with a sum energy corresponding to the Q value of the nuclear transition. A potential evidence has been claimed for the $0\nu\beta\beta$ mode of ^{76}Ge with $T_{1/2}^{0\nu} = 2.23^{+0.44}_{-0.31} \times 10^{25}\ yr$ at 90% CL [16,17].

Experimentally observed in 11 nuclides [18,19] is the standard model process of neutrino-accompanied double-β decay:

$$(Z, A) \rightarrow (Z + 2, A) + 2e^- + 2\nu_e \quad (2\nu\beta\beta), \tag{3}$$

which is expected with half-lives around 10^{20} yr depending on the Q value. For recent reviews, see Ref. [20]. An alternative process is the double-positron decay in combination with electron capture (EC). Three different decay modes can be considered:

$$(Z, A) \rightarrow (Z - 2, A) + 2e^+ + (2\nu_e) \quad (\beta^+\beta^+), \tag{4}$$

$$e^- + (Z, A) \rightarrow (Z - 2, A) + e^+ + (2\nu_e) \quad (\beta^+/\mathrm{EC}), \tag{5}$$

$$2e^- + (Z, A) \rightarrow (Z - 2, A) + (2\nu_e) \quad (\mathrm{EC/EC}). \tag{6}$$

Decay modes containing a positron have a reduced Q value because each generated positron accounts for a reduction of $2\ m_e c^2$ and thus can only occur in nuclides with sufficient

*bjoern.lehnert@tu-dresden.de
†zuber@physik.tu-dresden.de
‡erica.andreotti@ec.europa.eu
§mikael.hult@ec.europa.eu

energy difference from the daughter nuclide. The full energy is only available in the EC/EC mode, which makes it the most probable one; however, it is also the most difficult to detect, only producing x rays instead of 511-keV γ's.

Another set of searches focuses on excited-state transitions in double-β decays. This is experimentally interesting because the event topology is enhanced by deexcitation γ's, which are accessible with γ-ray spectroscopy. However, without information about the other final state particles, this technique cannot distinguish between the $0\nu\beta\beta$ mode and the $2\nu\beta\beta$ mode; hence, the deduced half-lives are valid for both. The investigation of $2\nu\beta\beta$ modes into excited states provides information on nuclear structure that is valuable for matrix element calculations. The understanding and tuning of parameters in matrix elements for $2\nu\beta\beta$ modes is imperative for translating the measured half-life of $0\nu\beta\beta$ experiments into a Majorana neutrino mass [Eq. (2)]. So far only transitions to the first-excited 0^+ state have been observed in ^{100}Mo [21] and ^{150}Nd [22]. The searches described in this paper are searches for excited-state transitions in palladium with γ-ray spectroscopy.

II. DOUBLE-β DECAYS IN PALLADIUM

The element under study is palladium with the isotopes of interest being ^{110}Pd and ^{102}Pd. Among the 35 isotopes expected to undergo $\beta^-\beta^-$ decay, ^{110}Pd has the second-highest natural abundance with 11.72%. Recently, the Q value was remeasured to 2017.85(64) keV [23] and this places ^{110}Pd among the 11 $\beta^-\beta^-$ isotopes with a Q value larger than 2000 keV. Two measurements of ^{110}Pd have been performed in the past in 1952 [24] and more recently in 2011 [25]. The latter measurement was the first to investigate excited states in palladium and is the direct predecessor of this search. There exist many theoretical calculations for transitions into the ground state and into the 2_1^+, 0_1^+, 2_2^+, 0_2^+, and 2_3^+ excited states to which the experimental limits can be compared. The existing experimental and theoretical half-life limits ares summarized in Table I. This paper aims to provide experimental information about every decay mode into excited states in ^{110}Pd and ^{102}Pd that has been investigated theoretically. Furthermore, ^{110}Pd is an excellent candidate to probe the single-state dominance hypothesis for $2\nu\beta\beta$ decay, i.e., that only the lowest-lying intermediate 1^+ state will contribute to the nuclear transition matrix element describing its $2\nu\beta\beta$ decay.

The second isotope ^{102}Pd has a Q value of 1172 keV, a natural abundance of 1.02%, and is able to decay via EC/EC and β^+/EC. The only experimental half-life limit is quoted in Ref. [25] and no theoretical calculation is published up to date. A summary can be found in Table II.

The search is based on γ spectroscopy; hence only γ lines are considered in the event topology. Each excited-state transition is followed by a unique set of decay branches and γ cascades, which are illustrated in Figs. 1 and 2.

III. EXPERIMENT

A. Measuring setup

The measurements were performed at the High Activity Disposal Experimental Site (HADES) underground laboratory on the premises of the Belgian Nuclear Research Centre SCK·CEN in Mol, Belgium. The underground laboratory is

TABLE I. Experimental and theoretical half-life limits for various $\beta\beta$-decay modes in ^{110}Pd. The columns show from left to right the theoretical model, the quoted half-life, the reference, and the year of publication. Abbreviations are denote as follows: PHFM, projected Hartree-Fock-Bogoliubov; SSDH, single-state-dominance hypothesis; SRPA, second quasi-random-phase approximation; OEM, operator expansion method; QRPA, quasi-random- phase approximation; SSD, single-state dominance; and *pn*QRPA, proton-neutron quasiparticle random-phase approximation.

Expt./Th. model	Lower limit $T_{1/2}$ (yr)	Reference	Year of publication
^{110}Pd ground-state transition			
Expt.	1×10^{17} (68% CL)	[24]	1952
PHFM	1.41×10^{20} and 3.44×10^{20}[a]	[26]	2005
SSDH	1.75×10^{20}	[27]	2000
SSDH	1.2–1.8×10^{20}[b]	[28]	1998
SRPA	1.6×10^{20}	[29]	1994
OEM	1.24×10^{21}	[30]	1994
QRPA	1.16×10^{19}	[31]	1990
SSD	1.2×10^{20}	[32]	2005
*pn*QRPA	1.1×10^{20} and 0.91×10^{20}[c]	[33]	2011
^{110}Pd 2_1^+ excited-state transition @ 657.76 keV			
Expt.	4.40×10^{19}(95% CL)	[25]	2011
SSD	4.4×10^{25}	[32]	2005
SRPA	8.37×10^{25}	[29]	1994
*pn*QRPA	1.48×10^{25}	[34]	2007
*pn*QRPA	0.62×10^{25} and 1.3×10^{25}[c]	[33]	2011
^{110}Pd 0_1^+ excitedstate transition @ 1473.12 keV			
Expt.	5.89×10^{19} (95% CL)	[25]	2011
SSD	2.4×10^{26}	[32]	2005
*pn*QRPA	4.2×10^{23} and 9.1×10^{23}[c]	[33]	2011
^{110}Pd 2_2^+ excited-State transition @ 1475.80 keV			
SSD	3.8×10^{31}	[32]	2005
*pn*QRPA	11×10^{30} and 7.4×10^{30}[c]	[33]	2011
^{110}Pd 0_2^+ excited-State transition @ 1731.33 keV			
SSD	5.3×10^{29}	[32]	2005
^{110}Pd 2_3^+ excited-State transition @ 1783.48 keV			
SSD	1.3×10^{35}	[32]	2005

[a] $g_A = 1.25$ and 1.0, respectively.
[b] Different experimental input for calculations.
[c] For Woods-Saxon potential and adjusted base, respectively (see Ref. [33] for details).

TABLE II. Experimental half-life limits for various EC/EC and β^+/EC decay modes in ^{102}Pd.

Expt./Th. model	Lower limit $T_{1/2}$(yr)	Reference	Year of publication
^{102}Pd 2_1^+ excited-state transition @ 475.10 keV			
Expt.	2.68×10^{18} (95% CL)	[25]	2011
^{102}Pd 0_1^+ excited-state transition @ 943.69 keV			
Expt.	7.64×10^{18} (95% CL)	[25]	2011

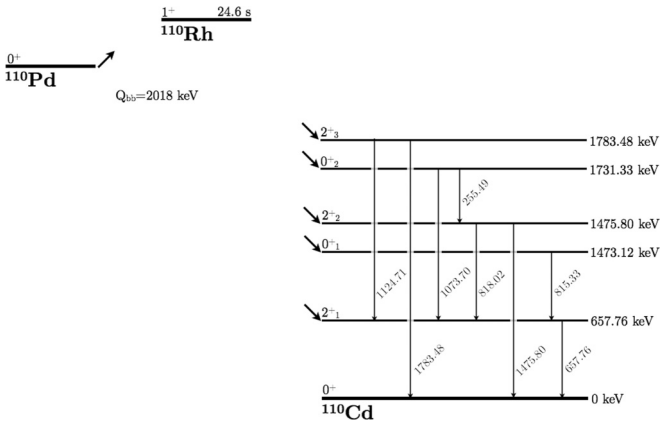

FIG. 1. ^{110}Pd level scheme of investigated decay modes. Nuclear data are from Ref. [35].

located at a depth of 225 m inside the Boom clay formation and has a flat overburden that amounts to roughly 500 m water equivalent [36].

The detector setup consists of two high-purity germanium (HPGe) detectors in a sandwich configuration with integrated muon veto panels on the top [37]. It is shown in Fig. 3. The sample is placed between the top (Ge-7) and bottom (Ge-6) detector. The distance between the two can be adjusted to maximize the solid angle acceptance and the detection efficiency. Ge-6 is a p-type HPGe detector with 80% efficiency and 0.9-mm dead layer in a 102-mm cryostat with a Cu endcap, whereas Ge-7 is an extended range p-type HPGe detector with 90% efficiency and a 0.3-μm dead layer in an Al cryostat. The characteristics of the Ge-7 detector makes it suitable for the detection of low-energetic x rays while the configuration of the Ge-6 detector has the advantage of reducing the background and x-ray coincidences. The shielding consists of an outer layer of 14.5-cm 20 Bq/kg (^{210}Pb) lead, an intermediate layer of 4.0-cm 2.4 Bq/kg (^{210}Pb) low-activity lead, and an inner layer of 3.5-cm electrolytic copper with less than 15 μBq/kg ^{60}Co and less than 20 μBq/kg ^{228}Th [37].

The data acquisition (DAQ) is twofold. The main DAQ, the DAQ2000 multi parameter system, is self-fabricated by the Institute for Reference Materials and Measurements (IRMM) and is recording events in list mode from the two

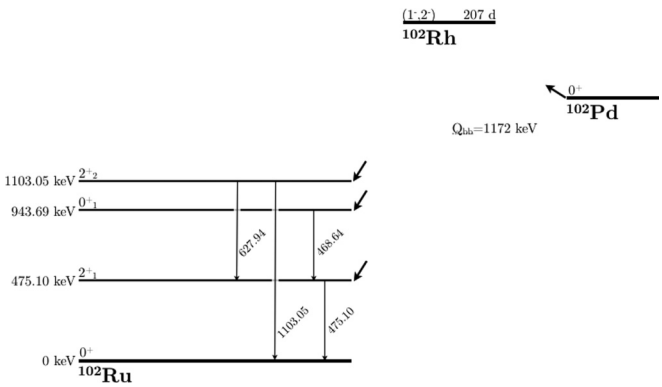

FIG. 2. ^{102}Pd level scheme of investigated decay modes. Nuclear data are from Ref. [35].

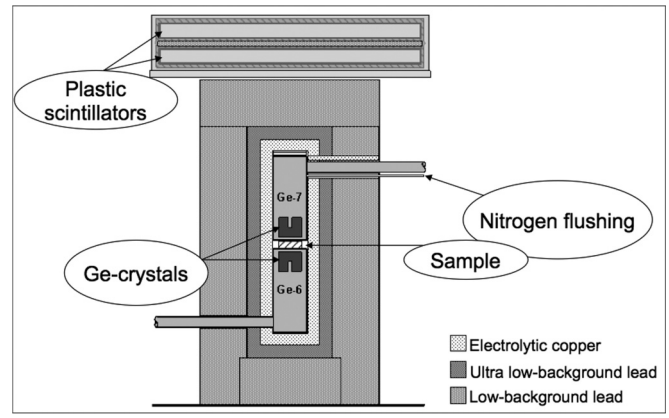

FIG. 3. IRMM germanium detector sandwich setup.

HPGe detectors as well as from the two muon panels which enables coincidence analysis in the ROOT framework [38]. Additionally, a standard GENIE DAQ system is used in histogram mode for each HPGe detector redundantly. The DAQ2000 was only operative for a reduced measuring time with limited sample exposure; thus the analysis in this work is performed with the GENIE DAQ and without muon veto or detector coincidence.

The total background rate in the germanium detectors was previously measured with 992 cts/d in an energy range of 40–2400 keV of which 124 cts/d were identified as muon events [37].

B. Palladium sample

Irregular shaped 1 mm $\times$ 1 cm^2 plates of palladium (802.35 g) were placed inside a measuring container of 70 mm in diameter and 50 mm in height. The plates were piled inside the container as dense as possible and an effective density of 10.2 g/cm^3 was calculated. The palladium was approximated with a homogeneous distribution and the effective density in the simulations for determining the detection efficiency. Recently, the sample was purified by C. HAFNER GmbH + Co. KG in 2010 to a certified purity of >99.95%, which lowered the continuous background in the peak regions by approximately 20% [25]. To avoid radionuclides produced by cosmic ray spallation, the palladium was kept underground and exposed only 18 d during purification in 2010 and 3 d for transport in the fall of 2011. A picture of the palladium sample before and after purification is shown in Fig. 4.

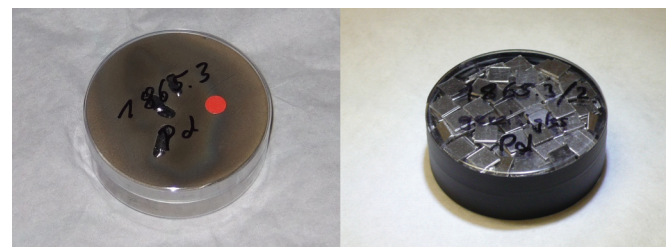

FIG. 4. (Color online) Palladium sample before (left panel) and after (right panel) purification inside the measuring container.

IV. ANALYSIS

A. Stability check

The histogram data of the GENIE DAQ was separated into individual runs of roughly 24 h for each of the two detectors Ge-6 and Ge-7. This enabled the stability check of the DAQ system over the extended period of measurement and the removal of individual runs.

The stability was checked by plotting the count rate and the peak centroid of the background peaks at 609 and 2614 keV as a function of time (spectrum number). Although counting statistics prevented detailed analysis of the short-term stability, it was clear that there was no measurable energy drift during the measurement period. In addition, quality controls with a point source containing ^{60}Co, ^{137}Cs, and ^{241}Am were carried out before, after, and once in-between the measurement. The average ^{222}Rn activity concentration in the laboratory during the data taking was measured to 9.5 Bq/m^3 and at no point higher than 25 Bq/m^3. No correlation to the background count rate was observed mainly due to effective Rn removal by minimizing empty space inside the shield and flushing with N_2. The count rate remained stable over the 32 runs with one exception; in the first two runs an increase in total counts and counts from ^{208}Tl was observed, however not from ^{214}Bi. This behavior was cross-checked with additional visible γ lines from 583.19-keV ^{208}Tl and 239.63-keV ^{212}Pb, and 1764.49-keV ^{214}Bi representing the ^{232}Th and ^{238}U decay chains, respectively. The increased count rate of the ^{232}Th chain in the first days is only seen in the lower Ge-6 detector with a Cu endcap and not in the upper Ge-7 detector with an Al endcap. One possible explanation is that the short half-life of ^{220}Rn (55.6 s) implies that it is not flushed out by boil-off nitrogen and that its daughters preferentially stick to the copper surface of the lower detector (Ge-6) rather than to the aluminum surface of the upper detector (Ge-7). ^{222}Rn with a longer half-life (3.8 d) will be flushed out of the shield before a significant number of daughters are produced. Consequently, the first two runs are removed from the analysis resulting in a total of 30 runs with 44.77 d of good data out of 32 runs with 46.49 d total data, which translates into a total exposure of 35.92 kg/d.

B. Data processing

For the final analysis a single energy spectrum is used in which all individual runs are summed: In a first step, all selected runs of one detector are combined with the same energy calibration. In a second step, the single detector spectra are rebinned into a common binning of 0.5 keV/bin and a common energy range from 20 to 2720 keV. Additionally, the Ge-6 spectrum is scaled to the lifetime of the Ge-7 spectrum, which becomes the common lifetime of the sum spectrum. The commonly binned and scaled spectra are added. These steps result in a noninteger sum spectrum that denotes the count per bin in the lifetime of Ge-7. The difference in lifetime between the two detectors is less than 0.5% for the selected runs. The combined spectrum of Ge-6 and Ge-7 together with a background spectrum of 13.62 d is shown in Fig. 5.

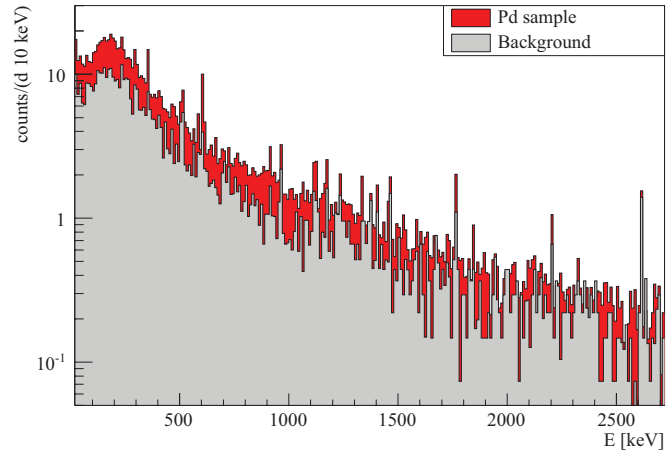

FIG. 5. (Color online) Sum spectrum of Ge-6 and Ge-7 detectors for a selected data set (44.77 d) in red and a background spectrum (13.62 d) in gray. The spectra are shown in common 10-keV bins between 20 and 2720 keV.

C. Background investigation

The radiopurity of the palladium sample was assessed during the γ-spectrometry measurement performed at HADES. In the measured spectrum, the major γ lines emitted by natural radionuclides belonging to the ^{238}U and ^{232}Th chains and to ^{40}K as well as the ^{60}Co lines are visible. The palladium spectrum is compared to the background spectrum measured without a sample. The background peak count rate is subtracted from that of the palladium sample. The result, if positive, is then used for the evaluation of the activity due to the impurities in the sample. In case of a negative result, a decision threshold is calculated according to Ref. [39]. The results are reported in Table III. Decision thresholds are also calculated for the following radionuclides: ^{102}Rh ($T_{\frac{1}{2}} = 207.3$ d), ^{102m}Rh ($T_{1/2} = 3.742$ yr), and ^{110m}Ag ($T_{1/2} = 249.76$ d). The reason is the possible interference with the search for ^{110}Pd and ^{102}Pd isotopes, because of the emission of γ lines from the same excited daughter states. No presence of these radionuclides is found, as reported in Table IV.

D. Peak finding

The analysis is a peak search on the detector sum spectrum and either retrieves the number of counts in a respective peak or states an upper limit of counts according to a level of confidence. In an experiment with non-negligible background, the background can fluctuate upwards or downwards. The sensitivity of an experiment is then defined as a resulting signal which originates from a 1 σ upward fluctuation of the background. This can be calculated before performing the experiment if the background is known. In the case of the observation of a downward fluctuation, which formally results in negative signal counts, the signal is usually set to zero and the sensitivity is quoted as an upper limit of the counts. On the other hand, when using classical uncertainties on the observed downward fluctuated counts, it is possible that in some cases even the upper limit is negative. In these cases it results in a poor coverage of the quoted confidence level at best and in

TABLE III. Massic activities (in mBq/kg) of radioimpurities detected in the Pd sample.

Nuclide	E (keV)	Massic activity (mBq/kg)	Decision threshold ($\alpha = 95\%$) (mBq/kg)	Weighted mean massic activity (mBq/kg)
^{214}Pb	295.22	1.9 ± 1.0	1.4	1.4 ± 0.4
	351.93	1.3 ± 0.5	0.6	
^{214}Bi	609.32	1.9 ± 0.4	0.4	1.9 ± 0.4
	1120.29	2.0 ± 0.8	0.9	
	1238.11	—	2.2	
	1377.67	—	2.7	
	1764.54	—	3.2	
^{210}Pb	46.54	—	414.3	
^{228}Ac	911.20	—	0.5	
	968.97	—	0.9	
^{212}Pb	238.63	—	0.7	
^{208}Tl	583.19	—	0.6	
	2614.51	—	0.3	
^{40}K	1460.82	—	1.0	
^{137}Cs	661.66	—	0.2	
^{60}Co	1173.23	—	0.2	
	1332.49	—	0.1	

an unphysical negative result at worst. Additionally there is a discontinuity in the coverage when crossing from a two-sided confidence interval definition to a one-sided one.

All these problems are addressed by the method of Feldman and Cousins in their paper [40]. They use a Neyman construction of a confident belt and an ordering principle based on likelihood ratios. The advantages are a physical yield in all background situations, i.e., a positive upper count limit and avoiding discontinuities in the coverage while crossing the statistical interpretation from a nonobservation to an observation, i.e., from a one-sided to a two-sided confidence interval. The confidence intervals of the Feldman-Cousins method are believed to have a better coverage for small numbers than Gaussian ones [40].

No prominent peak structures are observed in the signal region and the results of the analysis are upper limits only for the peak counts. To obtain a numerical value, all bins within a peak are combined into a single analysis bin that covers at least the full width at half maxium of the peak. The real

TABLE IV. Decision thresholds for direct γ background of double-β-decay intermediate nuclei.

Nuclide	E (keV)	Decision threshold ($\alpha = 95\%$) (mBq/kg)
^{110m}Ag	1384.30	0.5
	1505.04	1.0
^{102}Rh	475.05	0.4
^{102m}Rh	631.28	0.3
	697.49	0.3

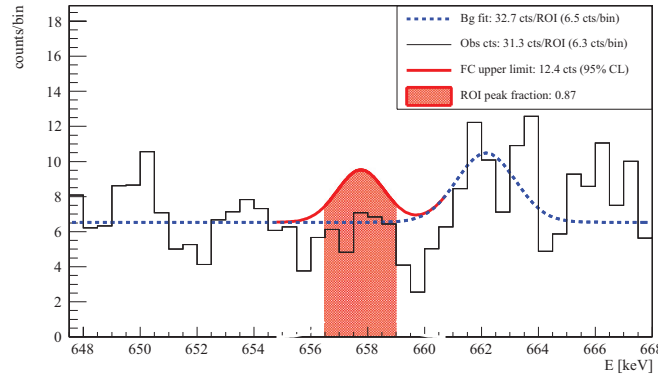

FIG. 6. (Color online) The peak region around the 657.76-keV γ line from ^{110}Pd and the 661.66-keV γ line from ^{137}Cs.

signal fraction coverage is calculated as the Gaussian peak area in the analysis bin and depends on the actual binning of the spectrum. The peak background is fitted with a constant function defined ± 30 keV around the peak energy excluding a window of ± 5 keV around the peak. In the case of prominent background peaks in the side bands, they are included in the background function as Gaussians. This was done for the background peaks at 609.31, 1120.29, and 1764.49 keV from ^{214}Bi, at 238.63 keV from ^{212}Pb, at 1461.83 keV from ^{40}K, and at 661.66 keV from ^{137}Cs. In the case of the 661.66-keV peak which is close to the 657.76-keV peak in the ^{110}Pd system, the flat background function was defined closer than ± 5 keV into the signal region to improve the background estimation.

The observed counts in the analysis bin are compared to the expected background with the ROOT class TFeldmanCousins, which returns the lower and upper bound of the signal confidence interval according to a specified confidence level that is set to 95% in this work. All investigated peaks show a lower count limit of zero; this is in agreement with a nonobservation of the peak. To account for the incomplete coverage of the peak area by the analysis bin, the upper count limit is divided by the fraction of coverage and thus adjusts the upper count limit in a conservative way.

An illustration of the technique is shown in Figs. 6 to 9 with the energy spectrum in the solid black line, the background function in the dashed blue line, the peak fraction marked as

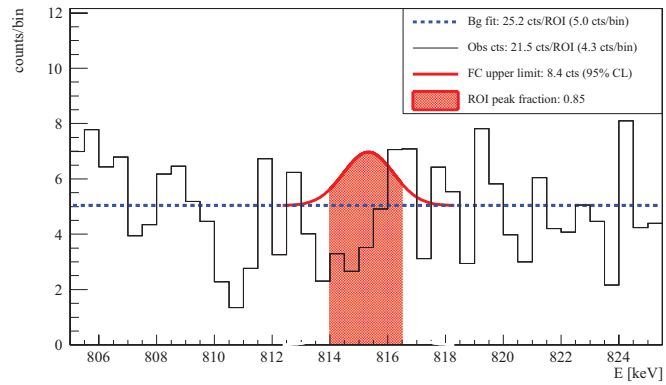

FIG. 7. (Color online) The peak region around the 815.33-keV γ line from ^{110}Pd 0_1^+.

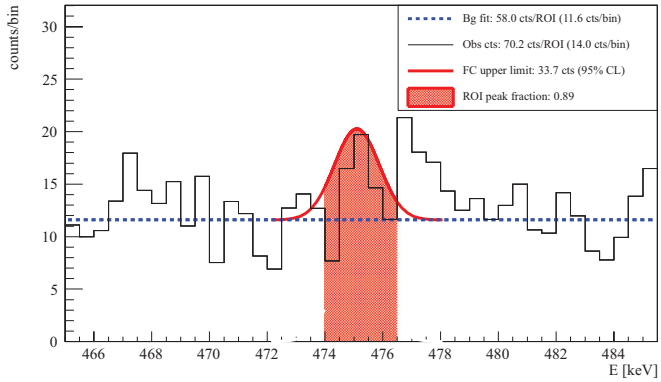

FIG. 8. (Color online) The peak region around the 475.10-keV γ line from ^{102}Pd 2_1^+.

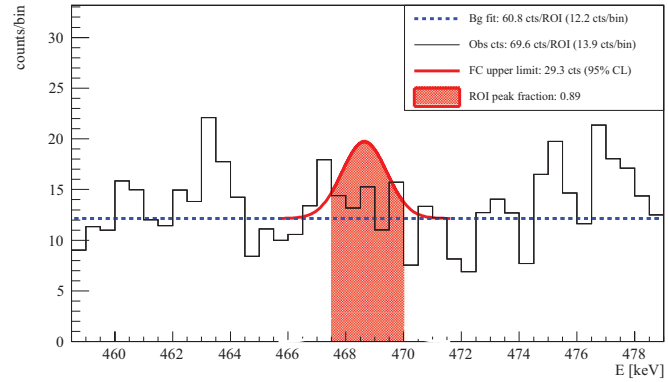

FIG. 9. (Color online) The peak region around the 468.64-keV γ line from ^{102}Pd 0_1^+.

the solid red area and the gaussian signal peak as it appears with the Feldman Cousins upper limit as the red solid line. The Feldman and Cousins limits are cross-checked with the International Organization for Standardization (ISO) standard methods [39] and agree better than within a factor of 2 with each other; this can be explained by the different treatment of statistical background fluctuations.

E. Monte Carlo simulation for γ line efficiencies

The full-energy peak (FEP) efficiencies were determined using Monte Carlo simulations with the EGS4 software. The models of the detectors were first determined from manufacturer data and using information from radiography. Thereafter the dead layer thicknesses were adjusted in the model to agree with measured FEP efficiencies from point sources within 3%. The final model was validated using volume sources of a size similar to that of the Pd source in this study. Each decay branch was simulated separately with information from Ref. [35] and the calculations involved all the cascading γ rays of each branch so that the resulting FEP efficiency was inherently corrected for the coincidence summing effect. X-ray coincidences and the angular correlations were neglected in

TABLE V. Experimental results for each decay mode and γ line. The columns from left to right denote the decay mode, the γ line energy, the emission probability in %, and the detection efficiency in %. The last two columns show the upper signal count limit and the deduced lower half-life limit at 95% CL.

Decay mode	γ line energy (keV)	Emission probability	Detection efficiency	Signal count limit	$T_{1/2}$ limit (yr)
^{110}Pd 2_1^+ 657.76 keV	657.76 keV	100%	4.70%	12.4	1.72×10^{20}
^{110}Pd 0_1^+ 1473.12 keV	815.33 keV	100%	3.84%	8.4	1.98×10^{20}
	657.76 keV	100%	3.94%	12.4	1.44×10^{20}
^{110}Pd 2_2^+ 1475.80 keV	1475.80 keV	35.25%	1.32%	11.5	5.17×10^{19}
	818.02 keV	64.75%	2.40%	16.3	6.67×10^{19}
	657.76 keV	64.75%	2.53%	12.4	9.26×10^{19}
^{110}Pd 0_2^+ 1731.33 keV	1073.7 keV	86.73%	1.89%	10.1	8.50×10^{19}
	657.76 keV[a]	95.32%	3.78%	12.4	1.38×10^{20}
	255.49 keV	13.27%	0.36%	25.3	6.46×10^{18}
	1475.80 keV	4.68%	0.12%	11.5	4.87×10^{18}
	818.02 keV	8.59%	0.24%	16.3	6.63×10^{18}
^{110}Pd 2_3^+ 1783.48 keV	1783.48 keV	21.57%	0.88%	6.2	6.45×10^{19}
	1125.71 keV	78.43%	2.48%	12.0	9.41×10^{19}
	657.76 keV	78.43%	2.99%	12.4	1.09×10^{20}
^{102}Pd 2_1^+ 475.10 keV	475.10 keV	100%	5.09%	33.7	5.95×10^{18}
^{102}Pd 0_1^+ 943.69 keV	468.64 keV	100%	4.32%	29.3	5.81×10^{18}
	475.10 keV	100%	4.31 %	33.7	5.04×10^{18}
^{102}Pd 2_2^+ 1103.05 keV	1103.05 keV	37.11%	1.60%	13.5	4.66×10^{18}
	627.94 keV	62.90%	2.54%	11.7	8.55×10^{18}
	475.10 keV	62.90%	2.67%	33.7	3.13×10^{18}

[a]This γ line is part of two sub-branches starting from the same excited state.

TABLE VI. Summary of measured half-life limits for all ^{110}Pd and ^{102}Pd double-β-decay excited-state transitions.

Decay mode	$T_{1/2}$ limit (yr) (95%)
^{110}Pd 2_1^+ 657.76 keV	1.72×10^{20}
^{110}Pd 0_1^+ 1473.12 keV	1.98×10^{20}
^{110}Pd 2_2^+ 1475.80 keV	9.26×10^{19}
^{110}Pd 0_2^+ 1731.33 keV	1.38×10^{20}
^{110}Pd 2_3^+ 1783.48 keV	1.09×10^{20}
^{102}Pd 2_1^+ 475.10 keV	5.95×10^{18}
^{102}Pd 0_1^+ 943.69 keV	5.81×10^{18}
^{102}Pd 2_2^+ 1103.05 keV	8.55×10^{18}

the simulations and it was assumed that the activity was homogeneously distributed in the whole volume of the sample.

V. RESULTS

All γ lines participating in a γ cascade were investigated and a half-life was calculated for each. Intrinsically, the calculation of limits is influenced by statistical fluctuations in the experimental spectrum; hence the largest calculated limit for an excited-state transition is quoted as the half-life limit of this transition. A summary of all investigated γ lines can be found in Table V: Quoted are the emission probability, the detection efficiency including summation effects, the upper count limit in the spectrum, and the calculated half-life. The selected half-life for each transition is listed in Table VI. The peak regions for the γ lines originating from the favored 0_1^+ transitions are shown in Figs. 6 and 7 for ^{110}Pd and in Figs. 8 and 9 for ^{102}Pd.

VI. CONCLUSION

A palladium sample has been investigated for double-β-decay transitions into excited states at the low background laboratory HADES. Lower half-life limits could be improved for the 0_1^+ and 2_1^+ transitions in ^{110}Pd and ^{102}Pd and first limits were established for all possible higher-energetic excited-state transitions. The best limit could be set for the ^{110}Pd 0_1^+ transition with a half-life larger than 1.98×10^{20} yr. The largest improvement compared to previous results was archived for the ^{110}Pd 2_1^+ transition with 1.72×10^{20} yr, which is an improvement by a factor of 3.9. For the ^{102}Pd system, the improvements were smaller due to upward fluctuations of the background in the peak region of the 475.10- and 468.64-keV γ lines.

Possible improvement of the search of double-β decays in palladium could be achieved by the consideration of x rays. This would require a different geometric assembly of the palladium plates, e.g., in a layer around an n-type HPGe detector with a thin dead layer. Further improvement could be achieved by considering γ coincidences using the multi-parameter DAQ system. This would also reduce the muonic background. The intrinsic massic activity of the palladium sample was determined to be 1.7 mBq/kg for the ^{238}U chain and below the detection threshold for the ^{232}Th chain. Further purifications are not expected to yield significant improvement. However, accumulating storage underground will reduce the general background from cosmic-activated radio isotopes in the palladium sample and the measuring system.

ACKNOWLEDGMENT

Gerd Marissens is acknowledged for extensive technical support. Furthermore the support of the HADES staff of EURIDICE is acknowledged.

[1] K. Abe *et al.* (Super-Kamiokande Collaboration), Phys. Rev. D **83**, 052010 (2011).
[2] B. Aharmim *et al.* (SNO Collaboration), arXiv:1109.0763.
[3] G. Alimonti *et al.* (BOREXINO Collaboration), Nucl. Instrum. Methods Phys. Rese., Sect. A **600**, 568 (2009).
[4] S. Hatakeyama *et al.*, Phys. Rev. Lett. **81**, 2016 (1998).
[5] J. K. Ahn *et al.* (RENO Collaboration), Phys. Rev. Lett. **108**, 191802 (2012).
[6] F. P. An *et al.* (Daya Bay Collaboration), Phys. Rev. Lett. **108**, 171803 (2012).
[7] S. Abe *et al.* (KamLAND Collaboration), Phys. Rev. Lett. **100**, 221803 (2008).
[8] F. Ardellier *et al.* (Double Chooz Collaboration), arXiv:hep-ex/0606025.
[9] P. Adamson *et al.* (MINOS Collaboration), Phys. Rev. Lett. **101**, 131802 (2008).
[10] K. Abe *et al.* (T2K Collaboration), Nuclear Instrum. Methods Phys Res., Sect. A **659**, 106 (2011).
[11] N. Agafonova *et al.* (OPERA Collaboration), New J. Phys. **14**, 033017 (2012).
[12] G. Mathews *et al.*, Phys. Rev. D **85**, 105023 (2012).
[13] J. Wolf, Nucl. Instrum. Methods Phys. Res., Sect. A **623**, 442 (2010).
[14] A. Monfardini *et al.* (MARE Collaboration), Nucl. Instrum. Methods Phys. Res., Sect. A **559**, 346 (2006).
[15] N. Jarosik *et al.*, Astrophys. J. Suppl. Ser. **192**, 14 (2011).
[16] H. Klapdor-Kleingrothaus, A. Dietz, H. Harney, and I. Krivosheina, Mod. Phys. Lett. A **16**, 2409 (2001).
[17] H. Klapdor-Kleingrothaus and I. Krivosheina, Mod. Phys. Lett. A **21**, 1547 (2006).
[18] V. I. Tretyak and Y. G. Zdesenko, At. Data Nucl. Data Tables **80**, 83 (2002).
[19] N. Ackerman *et al.* (EXO Collaboration), Phys. Rev. Lett. **107**, 212501 (2011).
[20] F. Avignone, S. Elliott, and J. Engel, Rev. Mod. Phys. **80**, 481 (2008).
[21] A. Barabash *et al.*, Phys. Lett. B **345**, 408 (1995).
[22] A. Barabash, F. Hubert, P. Hubert, and V. I. Umatov, Phys. At. Nucl. **67**, 1216 (2004).
[23] D. Fink *et al.*, Phys. Rev. Lett. **108**, 062502 (2012).
[24] R. Winter, Phys. Rev. **85**, 687 (1952).

[25] B. Lehnert and K. Zuber, Phys. Lett. B **705**, 47 (2011).
[26] R. Chandra *et al*., Eur. Phys. J. A **23**, 223 (2005).
[27] S. V. Semenov, F. Šimkovic, V. V. Khruschev, and P. Domin, Phys. At. Nucl. **63**, 1196 (2000).
[28] O. Civitarese and J. Suhonen, Phys. Rev. C **58**, 1535 (1998).
[29] S. Stoica, Phys. Rev. C **49**, 2240 (1994).
[30] M. Hirsch, X. Wu, H. Klapdor-Kleingrothaus, C. Cheng-rui, and H. Tso-hsiu, Phys. Rep. **242**, 403 (1994).
[31] A. Staudt, K. Muto, and H. V. Klapdor-Kleingrothaus, Europhys. Lett. **13**, 31 (1990).
[32] P. Domin, S. Kovalenko, F. Šimkovic, and S. Semenov, Nucl. Phys. A **753**, 337 (2005).
[33] J. Suhonen, Nucl. Phys. A **864**, 63 (2011).
[34] A. Raduta and C. Raduta, Phys. Lett. B **647**, 265 (2007).
[35] ENSDF database, http://www.nndc.bnl.gov/ensdf (July 10, 2012).
[36] E. Andreotti *et al*., in *the Proceedings of the 3rd International Conference on Current Problems in Nuclear Physics and Atomic Energy* (KINR, Kyiv, Ukraine, 2010).
[37] J. S. E. Wieslander *et al*., Appl. Radiat. Isot. **67**, 731 (2009).
[38] I. Antcheva *et al*., Comput. Phys. Commun. **180**, 2499 (2009).
[39] International Organization for Standardization, ISO 11929:2010 (2010).
[40] G. J. Feldman and R. D. Cousins, Phys. Rev. D **57**, 3873 (1998).